THE JOURNAL OF PHYSICAL CHEMISTRY A

Article

pubs.acs.org/JPCA

Evaluation of Interactions between Urokinase Plasminogen and Inhibitors Using Molecular Dynamic Simulation and Free-Energy Calculation

Rongjian Sa,† Liang Fang,† Mingdong Huang, Qiaohong Li, Yongqin Wei, and Kechen Wu*

State Key Laboratory of Structural Chemistry, Fujian Institute of Research on the Structure of Matter, 155 Yangqiao Road West, Fuzhou, Fujian 350002, People's Republic of China

ABSTRACT: The binding modes of urokinase-type plasminogen activator (uPA) with five inhibitors (1-(7-sulfonamidoisoquinolinyl) guanidine derivatives) were predicted based on molecular dynamic simulations. MM/PBSA free-energy calculations and MM/GBSA free-energy decomposition analyses were performed on the studied complexes. The calculated binding free energies are reasonably consistent with the experimental results. The free-energy decomposition analyses elucidate the different contributions of the energy of some favorable residues in the interactions between protein and ligand of each complex. The results indicate that the inhibitors mainly interact with the S1 pocket of uPA, wherein the hydrogen bonds and the interactions between guanidines and the corresponding residues play an important role. Moreover, hydrogen bond analyses show the water-mediated hydrogen-bond network near the S1 pocket between uPA, and the ligand probably leads to excellent selectivity of these inhibitors on uPA.

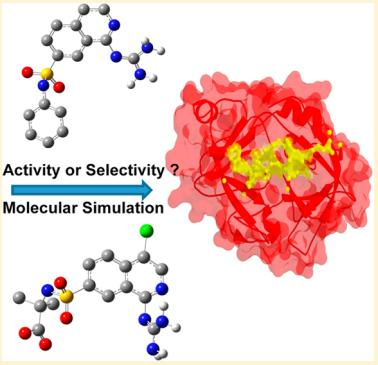

INTRODUCTION

Urokinase-type plasminogen activator (uPA) and its cognate receptor (uPAR) are involved in a number of physiopathological processes at the cell surface, including the regulation of plasminogen activation,[1] extracellular matrix remodeling,[2,3] growth-factor activation,[4] and the initiation of intracellular signaling.[5,6] The importance of the uPA system has been implicated in cellular invasion and tissue remodeling including cancer, atherosclerosis, bone remodeling, angiogenesis, tumor invasiveness, and spread of metastases.[7−9] The activity of uPA in affecting tumor progression has been extensive studied and demonstrated to be an effective target for cancer therapy.[7−12] Recently many inhibitors have been designed, not only for the inhibition of cancer, but also for a variety of other diseases associated with tissue remodeling.[7−13] There have been a number of crystal structures on uPA-inhibitor complexes described by several groups.[14−18]

The studies of X-ray structure on uPA-inhibitor complexes have provided a useful information for the design of uPA inhibitors.[7,8] Many efforts, both experimental and theoretical, have been devoted to searching for new inhibitors for several decades.[7−11] Many of these compounds are inhibitors for other serine proteases (e.g., thrombin, factor X, tPA, plasmin, trypsin) but with poor selectivity.[7−9] Thus, it is still a valuable target to search potent and selective inhibition of uPA over other serine proteases. Fish et al.[19] revealed a variety of potential and selective uPA inhibitors in their experimental research. These compounds were composed of sulfonamides and amines, which include an isoquinolinylguanidines with some groups substituting one hydrogen of sulfamide (Figure 1a−e). Furthermore, the binding mode of one uPA-inhibitor complex has been investigated by the X-ray crystallization studies. Because only one crystal structure of this series uPA-inhibitor complex is available, the further molecular dynamics (MD) simulation studies are helpful to achieve insight into the uPA−inhibitor binding interaction.

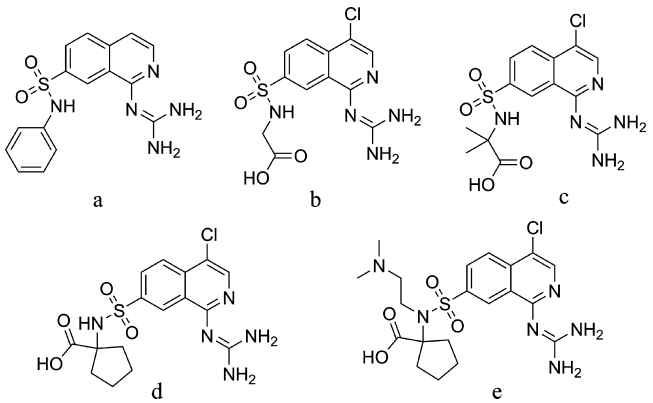

Figure 1. Reported chemical structures of five compounds: (a) compound **1**, (b) compound **2**, (c) compound **3**, (d) compound **4**, and (e) compound **5**.

The MD and binding free-energy calculations have been performed in this study on five uPA-inhibitor complexes (i) to testify whether free-energy calculation is a proper method for

Special Issue: International Conference on Theoretical and High Performance Computational Chemistry Symposium

Received: February 28, 2014
Revised: July 1, 2014
Published: July 1, 2014

   dx.doi.org/10.1021/jp5064319 | J. Phys. Chem. A 2014, 118, 9113−9119

uPA−inhibitor system, (ii) to explore the dynamic features of such interaction by MD simulation, and (iii) to understand the origin of the excellent activity and selectivity of these series inhibitors.

THEORETICAL METHODS

Molecular Dynamics Simulations. The initial models used in this paper were constructed on the basis of the X-ray crystal structure of uPA complex (PDB code: 2JDE).[19] The hydrogen atoms were added by using the Molecular Operating Environment modeling package (MOE 2007.09).[20] The crystallographic water molecules were deleted besides one crystallization water molecule near the active site S1 pocket.[19] The chemical structures of ligands 1−5 are shown in Figure 1a−e. The initial structures were first optimized by density functional theory method with B3LYP hybrid functional using 6-31G(d) basis sets accomplished by Gaussian03 package.[20] Then, the ligands were docked into uPA to generate the all-atom model of complexes using MOE.[21]

The ligand partial atomic charges were obtained by the B3LYP method and 6-31G (d) basis sets. The restrained electrostatic potential fit method[22] implemented in the antechamber module[23] of Amber10 software package[24] was used to fit the atom charges to the electrostatic potentials. Each model of complexes **1−5** was generated using LeaP module in Amber10. The MD calculations and the energy minimizations were carried out with Sander module in Amber10. The Amber ff99[25] and GAFF[26] parameters were applied to the protein residues and ligands, respectively. All ionizable residues were placed within their default protonation states with neutral pH value. The TIP3P water model[27] was used along each dimension with a margin of 10.0 Å. An appropriate number of Cl^- counterions were applied to neutralize the system. During the simulation, the SHAKE algorithm[28] was applied to constrain all covalent bonds to hydrogen atoms. The particle mesh Ewald method[29] was used for nonbond interaction with a 10.0 Å cutoff radius.

The following equilibration protocol was applied to the solvated models before the production phase. First, the harmonic constraints were applied to the complex using a restraint of weight of 500 kcal/(mol·Å^2). For the first 500 steps, the minimization of system energy was provided by the steepest descent method. Then, for the subsequent 4500 steps, the conjugated gradient method was employed to minimize the system energies. The NVT ensemble method was applied to obtain the stable state after the system was heated from 0 to 300 K over 50 ps in simulations. Subsequently, the whole solvated model was performed simulation without restraints for 1 ns. Finally, the NPT ensemble at 300 K and 1 atm was performed to a 4 ns production run. The coordinates were saved every 0.5 ps, and a time step of 1 fs was employed.

Binding Free-Energy Analysis. For each uPA−inhibitor complex, the binding free energies were calculated by the MM-PB (GB) SA approach.[30−33] 200 snapshots were selected from the last 1 ns trajectory with a 5 ps interval for further analysis. The counterions and the water molecules in this simulation were removed for free-energy calculations. The binding free energy between protein and ligand of every snapshot was estimated via eq 1.

$$\Delta G_{bind} = G_{complex} - [G_{protein} + G_{ligand}] \quad (1)$$

The free energies of the complex, the protein, and the ligand are characterized as $G_{complex}$, $G_{protein}$ and G_{ligand}, respectively. They can be calculated via eq 2.

$$\Delta G = \Delta G_{MM} + \Delta G_{sol} - T\Delta S \quad (2)$$

ΔG_{MM} is the free energy of molecular mechanics, ΔG_{sol} is the free energy of solvation, and $-T\Delta S$ represents the change in solute vibrational, rotational, and translational entropy. Considering the high computational cost and low prediction accuracy,[34,35] the contribution of the entropy was not considered in this calculation.

The free energy of molecular mechanics can be obtained by eq 3

$$\Delta G_{MM} = \Delta G_{ele} + \Delta G_{vdw} \quad (3)$$

where ΔG_{ele} is the electrostatic interaction, while ΔG_{vdw} is the interaction of van der Waals. The free energy of solvation is calculated by eq 4.

$$\Delta G_{sol} = \Delta G_{ele,sol} + \Delta G_{nonpol,sol} \quad (4)$$

$\Delta G_{ele,sol}$ represents the polar term to salvation and can be estimated by MM-PBSA[36] and MM-GBSA[37] methods. $\Delta G_{nonpol,sol}$ is the nonpolar solvation contribution and is determined as follows

$$\Delta G_{nonpol.sol} = \gamma SASA + b \quad (5)$$

where γ as the surface tension is set to 0.0072 kcal/(mol·Å^2)[38] and b is a constant equal to 0.[38] SASA is the solvent-accessible surface area (Å^2) that can be estimated by the linear combination of pairwise overlaps model.[39]

To elucidate the binding mode of the uPA and inhibitors, we decomposed the interaction energies into the binding free energies on a single residue by the MM-GBSA approach. Only the energies of the molecular mechanics and the solvation were applied to the free-energy decompositions in this calculation. The detailed procedure of MM-GBSA in our calculations is in accord with that of the MM-PBSA method.

RESULTS AND DISCUSSION

Stabilities of the Complexes. Figure 2a,b shows the root-mean-square deviation (RMSD) values of complexes **1−5** relative to the starting structures along the total simulation

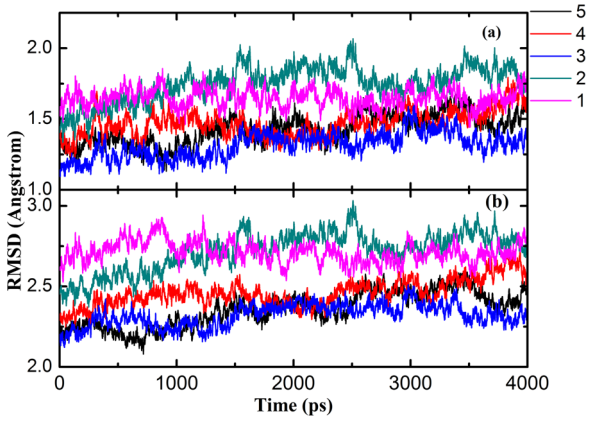

Figure 2. RMSD of (a) the protein backbone of and (B) all atoms of complexes **1−5** in the 4 ns MD simulations compared with the first coordinate frame. RMSD of (a) the protein backbone and (b) the ligands relative to the initial structures in the 4 ns MD simulations.

dx.doi.org/10.1021/jp5064319 | J. Phys. Chem. A 2014, 118, 9113−9119

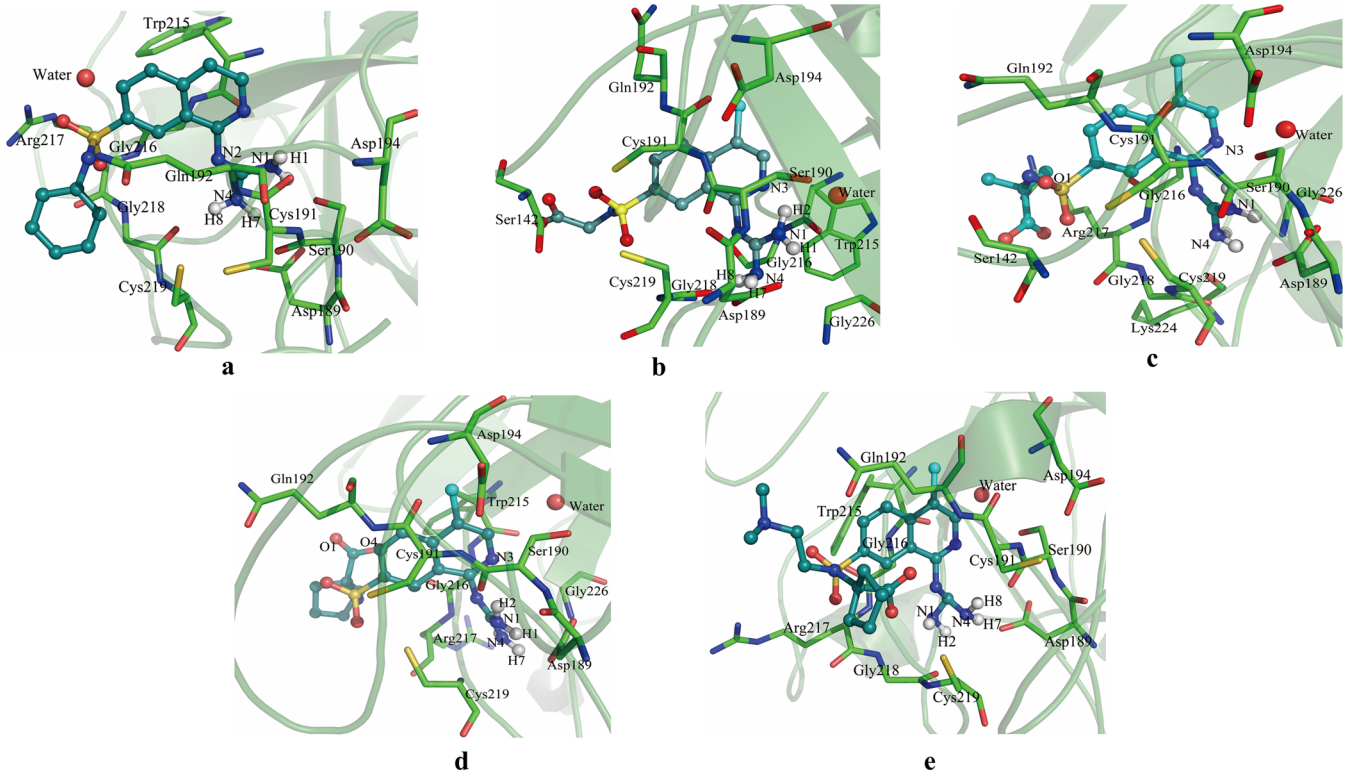

Figure 3. Structures of ligands and the crucial residues for five complexes: (a) complex **1**, (b) complex **2**, (c) complex **3**, (d) complex **4**, and (e) complex **5** in the last 1 ns simulation.

Table 1. Direct Hydrogen Bonds between uPA and the Ligand in Complexes 1−5

	direct hydrogen bonds						
	donor			acceptor		distance (Å)[a]	occupancy (%)[b]
1	ligand	H7	N4	Asp189	OD2	2.884	45.65
	Gly218	H	N	ligand	H8	3.009	37.35
	ligand	H8	N4	Asp189	OD2	2.892	33.50
	ligand	H1	N1	Ser190	OG	3.101	32.50
	Gly218	H	N	ligand	N2	3.259	32.35
2	ligand	H8	N4	Gly218	O	2.873	99.20
	ligand	H7	N4	Asp189	OD2	2.930	97.20
	ligand	H2	N1	Asp189	OD1	2.856	91.05
	ligand	H1	N1	Ser190	OG	2.946	63.30
	ligand	H7	N4	Asp189	OD1	3.260	61.70
3	ligand	H8	N4	Asp189	OD2	2.904	98.90
	ligand	H1	N1	Asp189	OD2	2.944	98.10
	ligand	H2	N1	Ser190	OG	3.010	88.40
	ligand	H1	N1	Asp189	OD1	3.175	63.40
	Gln192	HE22	NE2	ligand	O1	2.966	30.85
4	ligand	H1	N1	Asp189	OD2	2.847	98.60
	ligand	H7	N4	Asp189	OD2	3.093	79.60
	ligand	H2	N1	Ser190	O	2.890	62.70
	ligand	H1	N1	Asp189	OD1	3.137	53.15
	Gly216	H	N	ligand	O4	3.245	52.75
	Gln192	HE22	NE2	ligand	O1	2.931	34.20
5	ligand	H7	N4	Asp189	OD2	2.749	99.75
	ligand	H8	N4	Ser190	O	2.854	98.40
	ligand	H2	N1	Gly218	O	2.953	55.05

[a]Average distance between the acceptor and donor of hydrogen is in the analysis time period. [b]Occupancy is in units of percentage of the analysis time period. The H bond is defined by distance and angle. The hydrogen bond was defined as the combination of donor D, hydrogen H, and acceptor A atoms with a D−H···A configuration when the distance between donor D and acceptor A is shorter than 3.5 Å, and the angle A−H−D is larger than 120.0°.

dx.doi.org/10.1021/jp5064319 | J. Phys. Chem. A 2014, 118, 9113−9119

Table 2. Water-Mediated Hydrogen Bonds between uPA and the Ligand in Complex 2−5

	water-mediated hydrogen bonds						
	donor			acceptor		distance (Å)	occupancy (%)
2	Wat	H1	O	Val227	O	2.775	55.00
	Wat	H2	O	ligand	N3	3.023	50.45
	Wat	H2	O	Val227	O	2.773	38.80
	Wat	H1	O	ligand	N3	3.019	35.35
3	Wat	H2	O	Val227	O	2.820	45.00
	Wat	H1	O	Val227	O	2.830	38.15
	Ser190	HG	OG	Wat	O	2.946	31.60
	Wat	H1	O	ligand	N3	3.125	27.35
	Wat	H2	O	ligand	N3	3.130	18.55
4	Wat	H1	O	Val227	O	2.785	39.85
	Wat	H2	O	Val227	O	2.784	35.85
	Wat	H1	O	ligand	N3	3.248	8.60
	Wat	H2	O	ligand	N3	3.232	7.25
	Wat	H2	O	Ser190	OG	3.129	25.35
5	Wat	H1	O	Ser190	OG	3.114	24.60
	Wat	H2	O	Val227	O	2.871	20.30
	Wat	H1	O	Val227	O	2.898	18.40

Table 3. Binding Free-Energy Calculations for the Studied Complexes 1−5[b,a]

	ΔG_{ele}	ΔG_{vdw}	$\Delta G_{ele,polor}$	$\Delta G_{nopolor,sol}$	ΔG_{MM}	ΔG_{sol}	ΔG_{bind}	$\Delta G_{bind,exp}$
1	−33.65 ± 6.24	−38.48 ± 4.17	40.92 ± 3.86	−4.73 ± 0.30	−72.13 ± 7.99	36.19 ± 3.75	−35.95 ± 5.92	−39.03
2	−42.98 ± 6.52	−38.44 ± 3.19	47.98 ± 3.88	−4.46 ± 0.16	−81.43 ± 6.14	43.52 ± 3.86	−37.91 ± 3.65	−42.03
3	−33.62 ± 6.10	−42.85 ± 3.05	38.99 ± 4.49	−4.72 ± 0.18	−76.47 ± 6.15	34.27 ± 4.50	−42.20 ± 4.38	−45.94
4	−49.12 ± 7.13	−42.97 ± 3.79	53.66 ± 4.62	−4.91 ± 0.24	−92.09 ± 7.08	48.75 ± 4.57	−43.34 ± 4.14	−47.30
5	−49.53 ± 7.86	−47.87 ± 3.11	57.76 ± 5.76	−5.08 ± 0.22	−97.39 ± 8.25	52.68 ± 5.70	−44.71 ± 3.78	−49.30

[a]All energies are in kilocalories per mole. [b]ΔG_{ele}: electrostatic interaction. ΔG_{vdw}: interaction of van der Waals. $\Delta G_{ele,polor}$: contribution from polar to solvation. $\Delta G_{nopolor,sol}$: nonpolar contribution to solvation. $\Delta G_{MM} = \Delta G_{ele} + \Delta G_{vdw} + \Delta\Delta G_{nopolor,sol} + \Delta G_{nopolor,sol}$: binding free energy without entropic contribution. $\Delta G_{bind,exp}$: binding free energies data of experiment estimated as $RT \ln(IC50)$.[19]

trajectory to explore the stability of five uPA-inhibitor complexes during the simulation. For the entire complex, the atoms in protein only slightly deviate from the initial structures after 3 ns equilibration procedure. Then, all complexes tend to reach their stable states after such equilibration. Consequently, all energy data were collected, and analyses were obtained from the MD trajectory between 3 and 4 ns simulation procedure. The structures of five inhibitors and neighboring primary residues in complexes **1**−**5** after 4 ns simulation are shown in Figure 3a−e.

Hydrogen Bond Analysis. According to studies of Manas et al.,[40] the conserved amino acids that form hydrogen bonds with the inhibitor play an important role in the ligand−receptor binding. Therefore, we investigated the last 1 ns snapshots of the MD trajectory. Table 1 lists direct hydrogen bonds between uPA and the inhibitor over 30.0% occupancy. From the occupancy data, the hydrogen bonds strengthened in complexes **2**−**5** compared with complex **1**. In all complexes, the primary hydrogen bond interaction was the one formed between Asp189 and the terminal guanidine of ligand. Ser190 formed another important hydrogen bond connecting to the terminal guanidine of inhibitor. For **1**, **2**, and **5** complexes, a hydrogen bond was formed between Gly218 and the terminal guanidine of inhibitor, while for **3** and **4** complexes, a hydrogen bond was found between Gln192 and the oxygen of sulfonyl group. In addition, a hydrogen bond is formed between Gly216 and the oxygen of carboxylic in complex **4**. Table 2 lists the hydrogen bonds mediated by one water molecule between the uPA and the inhibitor. In complexes **2**, **3**, and **4**, the hydrogen bonding network was formed by one water molecule between Val227 and the ligand N3. Additionally, Ser190 participated in the hydrogen-bonding interaction in complex **3**. There is something different in complex **5** that no such a hydrogen-bonding network was found among uPA residues and the inhibitor in the setting range. This is attributed to the large distance between the ligand N3 and the water. Moreover, it should be noted that the water molecule in complex **1** moves out of the original position near the S1 pocket, so the similar hydrogen-bonding interaction between uPA residues and the inhibitor was not found. For all five systems, this water molecule in complexes was fully conserved during the entire MD calculation.

Analysis of Binding Free Energy. Table 3 showed the total binding free energy (ΔG_{bind}) and all other energy terms by MM-PBSA approach to compare the binding ability of these five inhibitors with uPA. The calculated ΔG_{bind} increased gradually from complexes **1** to **5**, which was in reasonable agreement with that derived from the experiment.[19] The results suggested that the energies of van der Waals and electrostatic made the major contribution to the binding, while the contributions of the energies of polar solvation were negative. The energies of nonpolar solvation slightly favorably contributed to the binding.

Table 3 showed that the van der Waals interaction energy between uPA residues and the ligand in complex **2** approximated to that in complex **1**, whereas the electrostatic energy of **2** was 9.33 kcal/mol larger than that of **1**. The solvation effect partially counteracted the favorable electrostatic

dx.doi.org/10.1021/jp5064319 | J. Phys. Chem. A 2014, 118, 9113−9119

Table 4. Energy Contributions (ΔG_{bind}) of the uPA Residues to the Binding of Each Ligand[a]

residue	1	2	3	4	5
ligand	−17.02 ± 2.97	−17.30 ± 2.16	−18.73 ± 2.70	−20.47 ± 2.50	−21.46 ± 2.19
Asp189	−2.41 ± 1.68	−3.52 ± 0.89	−5.57 ± 1.23	−4.15 ± 1.29	−5.78 ± 1.58
Ser190	−2.20 ± 2.49	−1.53 ± 0.86	−0.82 ± 1.00	−1.57 ± 1.06	−2.12 ± 0.93
Cys191	−1.53 ± 0.72	−1.72 ± 0.33	−1.53 ± 0.36	−1.58 ± 0.36	−1.74 ± 0.46
Gln192	−2.17 ± 0.99	−1.78 ± 0.84	−1.76 ± 0.86	−1.96 ± 0.91	−2.69 ± 0.59
Asp194	−0.51 ± 0.28	−0.85 ± 0.18	−0.64 ± 0.16	−0.92 ± 0.21	−0.65 ± 0.17
Trp215	−0.85 ± 1.04	−1.05 ± 0.53	−0.32 ± 0.74	−1.57 ± 0.73	−0.55 ± 0.82
Gly216	−1.44 ± 0.63	−0.63 ± 0.81	−0.86 ± 0.48	−2.73 ± 0.78	−1.2 ± 0.46
Arg217	−1.95 ± 1.11	−0.20 ± 0.27	−1.78 ± 0.83	−2.10 ± 0.50	−2.46 ± 1.01
Gly218	−1.26 ± 0.67	−2.38 ± 0.65	−1.42 ± 0.63	−0.45 ± 0.47	−1.71 ± 0.78
Cys219	−1.03 ± 0.81	−1.08 ± 0.51	−1.51 ± 0.65	−0.74 ± 0.76	−1.47 ± 0.65
Lys224	−0.15 ± 0.53	0.09 ± 0.04	−1.02 ± 0.49	−0.07 ± 0.25	−0.07 ± 0.27
Gly226	−0.31 ± 0.5	−0.64 ± 0.37	−0.95 ± 0.60	−1.84 ± 0.55	−0.35 ± 0.44
Ser142	−0.08 ± 0.43	−0.47 ± 0.56	−0.84 ± 0.54	0.03 ± 0.03	0

[a]All energies are in kilocalories per mole.

interactions. Thus, the difference in the electrostatic interactions decreased to 2.27 kcal/mol. As a result, the binding free energy of complex **2** was 1.96 kcal/mol larger than that of complex **1**. From complex **2** to **3**, the electrostatic energy decreased by 9.36 kcal/mol. However, the difference of electrostatic energy decreased to 0.11 kcal/mol by the effect of solvation. The calculated interaction energies of van der Waals between uPA and ligands **2**/**3** were −38.44 and −42.85 kcal/mol, respectively. Obviously, a large increase in van der Waals energy was caused by ligand **3**, which led to the increased binding affinity of complex **3**. From complexes **3** to **4**, the van der Waals energies change slightly. While in complex **4**, the electrostatic energy increased greatly, and the electrostatic interaction energies between uPA and ligands **3**/**4** were −33.62 and −49.12 kcal/mol, respectively. However, the solvation effect of complex **4** increased and partially counteracted the favorable electrostatic interactions. As a result, the binding free energy of complex **4** was 1.14 kcal/mol larger than that of complex **3**. In comparison with complex **4**, the electrostatic interaction energy of complex **5** had a small increase of 0.41 kcal/mol, and the van der Waals energy increased by 4.90 kcal/mol. However, the solvation effect was partially negative to the favorable interaction of van der Waals. Consequently, the binding free energy of complex **5** increased by 1.37 kcal/mol.

Decomposition of Free Energy. The MM-GBSA method was applied to elucidate the uPA-inhibitor interactions and the contribution of every residue. The energy contributions of some important residues in the uPA-inhibitor interactions are listed in Table 4. According to the predicted binding models of complexes **1** to **5** after 4 ns simulation shown in Figure 3a−e, the guanidine group in each compound moiety fits very well in the S1 pocket of uPA. Asp189 is the most energy favorable residue for the binding in all complexes. Besides, Ser190, Cys191, and Gln192 made large contributions to the binding free energies. Their total energy contributions were −8.31 kcal/mol (**1**), −8.65 kcal/mol (**2**), −9.68 kcal/mol (**3**), −9.26 kcal/mol (**4**), and −12.33 kcal/mol (**5**), respectively. Additionally, residues Trp215, Gly216, Arg217, Gly218, and Cys219 had considerable contributions that in total were −5.50 cal/mol (**1**), −4.26 kcal/mol (**2**), −5.89 kcal/mol (**3**), −6.60 kcal/mol (**4**), and −7.39 kcal/mol (**5**), respectively. It is notable that the energy contributions of residues Gly226 and Ser142 in complex **2** increased compared with those in complex **1**, and for complex **3**, the energy contributions of these residues enlarged further. In addition, Lys224 made notable contributions to the binding free energies. As for complex **4**, the interaction energies between Gly226 and ligand became comparatively larger. From another side of view, the contributions of ligand segments to the bindings were −17.02 (**1**), −17.3 (**2**), −18.73 (**3**), −20.47 (**4**), and −21.46 kcal/mol (**5**), respectively, which were in accord with the previously described binding free-energy analysis results.

CONCLUSIONS

In summary, we predicted the binding modes of uPA protease with five inhibitor molecules 1-(7-sulfonamidoisoquinolinyl)-guanidines based on MD simulations. We performed the MM/PBSA free-energy calculations and the MM/GBSA free-energy decomposition analyses on the studied complexes. The calculated results indicated that the binding free energies increased gradually from complexes **1** to **5**, which were in reasonable agreement with the experiment values. When the ligand changed from **1** to **2** and from **3** to **4**, the electrostatic interaction energies between uPA and the ligand increased obviously. When the ligand changed from **2** to **3** and from **4** to **5**, the van der Waals interactions between uPA and the ligand had a large increase. The residue ASP 189 makes the most favorable contribution to the binding free energy among these complexes. Besides, residues Ser190, Cys191, and Gln192 made big contributions to the binding free energies in all complexes. Additionally, residues TRP215, Gly216, Arg217, Gly218, and Cys219 had considerable contributions. Moreover, hydrogen-bond analysis showed that a hydrogen-bonding network was mediated by one water molecule among uPA Val227 and the nitrogen of the isoquinoline ring in **2**, **3**, and **4** complexes, which confirmed the assumption of the experiment that the water molecule near the active site S1 pocket contributes to the potency and selectivity of these inhibitors on uPA.

AUTHOR INFORMATION

Corresponding Author

*E-mail: wkc@fjirsm.ac.cn. Tel: 86-591-83792600.

Author Contributions

†R.S. and L.F. contributed equally to this work.

Notes

The authors declare no competing financial interest.

■ ACKNOWLEDGMENTS

R.J.S. thanks Prof. Weiliang Zhu and Drs. Weihua Li and Jian Zhang for their helpful discussions. We thank Dr. Dave Case for offering us the Amber program (http://ambermd.org). This work was supported by the NSFC (nos. 81001403, 91122015, 21171165, and 21201165) and the Institute Key Program (SZD08003) of FJIRSM.

■ REFERENCES

(1) Myohanen, H.; Vaheri, A. Regulation and Interactions in the Activation of Cell-Associated Plasminogen. *Cell. Mol. Life Sci.* **2004**, *61*, 2840−2858.
(2) Dano, K.; Romer, J.; Nielsen, B. S.; Bjorn, S.; Pyke, C.; Rygaard, J.; Lund, L. R. Cancer Invasion and Tissue Remodeling-Cooperation of Protease Systems and Cell Types. *APMIS* **1999**, *107*, 120−127.
(3) Behrendt, N. The Urokinase Receptor (uPAR) and the uPAR-Associated Protein (uPARAP/Endo180): Membrane Proteins Engaged in Matrix Turnover during Tissue Remodeling. *Biol. Chem.* **2004**, *385*, 103−136.
(4) Rabbani, S. A.; Mazar, A. P. The Role of the Plasminogen Activation System in Angiogenesis and Metastasis. *Surg. Oncol. Clin. North Am.* **2001**, *10*, 393−415.
(5) Blasi, F.; Carmeliet, P. uPAR: A Versatile Signalling Orchestrator. *Nat. Rev. Mol. Cell Biol.* **2002**, *3*, 932−943.
(6) Jo, M.; Thomas, K. S.; O'Donnell, D. M.; Gonias, S. L. Epidermal Growth Factor Receptor-Dependent and -Independent Cell-Signaling Pathways Originating from the Urokinase Receptor. *J. Biol. Chem.* **2003**, *278*, 1642−16646.
(7) Rockway, T. W.; Nienaber, V.; Giranda, V. L. Inhibitors of the Protease Domain of Urokinase-Type Plasminogen Activator. *Curr. Pharm. Des.* **2002**, *8*, 2541−2558.
(8) Rockway, T. W.; Giranda, V. L. Inhibitors of the Proteolytic Activity of Urokinase Type Plasminogen Activator. *Curr. Pharm. Des.* **2003**, *9*, 1483−1498.
(9) Duffy, M. J. The Urokinase Plasminogen Activation System: Role in Malignancy. *Curr. Pharm. Des.* **2004**, *10*, 39−49.
(10) Pillay, V.; Dass, C. R.; Choong, P. F. M. The Urokinase Plasminogen Activator Receptor as a Gene Therapy Target for Cancer. *Trends Biotechnol.* **2007**, *25*, 33−39.
(11) Bhongade, B. A.; Gadad, A. K. Insight into the Structural Requirements of Urokinase-Type Plasminogen Activator Inhibitors based on 3D QSAR CoMFA/CoMSIA Models. *J. Med. Chem.* **2006**, *49*, 475−489.
(12) Ulisse, S.; Baldini, E.; Sorrenti, S.; D'Armiento, M. The Urokinase Plasminogen Activator System: A Target for Anti-Cancer Therapy. *Curr. Cancer Drug Targets* **2009**, *9*, 32−71.
(13) Spraggon, G.; Phillips, C.; Nowak, U. K.; Ponting, C. P.; Saunders, D. The Crystal Structure of the Catalytic Domain of Human Urokinase-type Plasminogen Activator. *Structure* **1995**, *3*, 681−691.
(14) Nienaber, V. L.; Davidson, D.; Edalji, R.; Giranda, V. L.; Klinghofer, V. Structure-Directed Discovery of Potent Non-peptidic Inhibitors of Human Urokinase that Access a Novel Binding Subsite. *Structure* **2000**, *8*, 553−563.
(15) Katz, B. A.; Mackman, R.; Luong, C.; Radika, K.; Martelli, A. Structural Basis for Selectivity of a Small Molecule, S1-Binding, Submicromolar Inhibitor of Urokinase-type Plasminogen Activator. *Chem. Biol.* **2000**, *7*, 299−312.
(16) Nienaber, V.; Wang, J.; Davidson, D.; Henkin, J. Re-engineering of Human Urokinase Provides a System for Structure-Based Drug Design at High Resolution and Reveals a Novel Structural Subsite. *J. Biol. Chem.* **2000**, *275*, 7239−7248.
(17) Huai, Q.; Mazar, A. P.; Kuo, A.; Parry, G. C.; Shaw, D. E.; Callahan, J.; Li, Y.; Yuan, C.; Bian, C.; Chen, L.; et al. Structure of Human Urokinase Plasminogen Activator in Complex with its Receptor. *Science* **2006**, *311*, 656−659.
(18) Li, Y.; Parry, G.; Chen, L.; Callahan, J. A.; Shaw, D. E.; Meehan, E. J.; Mazar, A. P.; Huang, M. An Anti-Urokinase Plasminogen Activator Receptor (uPAR) Antibody: Crystal Structure and Binding Epitope. *J. Mol. Biol.* **2007**, *365*, 1117−1129.
(19) Fish, P. V.; Barber, C. G.; Brown, D. G.; Butt, R.; Collis, M. G.; Dickinson, R. P.; Henry, B. T.; Horne, V. A.; Huggins, J. P.; King, E.; et al. Selective Urokinase-Type Plasminogen Activator Inhibitors. 4. 1-(7-sulfonamidoisoquinolinyl) Guanidines. *J. Med. Chem.* **2007**, *50*, 2341−2351.
(20) Frisch, M. J.; Trucks, G. W.; Schlegel, H. B.; Scuseria, G. E.; Robb, M. A.; Cheeseman, J. R.; Montgomery, J. A., Jr.; Vreven, T.; Kudin, K. N.; Burant, J. C.; et al. *Gaussian 03*, revision D.01; Gaussian, Inc.: Wallingford, CT, 2004.
(21) *Molecular Operating Environment (MOE)*, version 2007.09; Chemical Computing Group, Inc.: Montreal, 2007.
(22) Cieplak, P.; Cornell, W. D.; Bayly, C.; Kollman, P. A. Application of the Multimolecule and Multiconformational RESP Methodology to Biopolymers: Charge Derivation for DNA, RNA and Proteins. *J. Comput. Chem.* **1995**, *16*, 1357−1377.
(23) Wang, J.; Wang, W.; Kollman, P. A.; Case, D. A. Automatic Atom Type and Bond Type Perception in Molecular Mechanical Calculations. *J. Mol. Graphics Modell.* **2006**, *25*, 247−260.
(24) Case, D. A.; Darden, T. A.; Cheatham, T. E., III; Simmerling, C. L.; Wang, J.; Duke, R. E.; Luo, R.; Merz, K. M.; Pearlman, D. A.; Crowley, M.; et al. *AMBER 10*; University of California: San Francisco, 2008.
(25) Wang, J.; Cieplak, P.; Kollman, P. A. How Well Does a Restrained Electrostatic Potential (RESP) Model Perform in Calculating Conformational Energies of Organic and Biological Molecules? *J. Comput. Chem.* **2000**, *21*, 1049−1074.
(26) Wang, J.; Wang, R. M.; Caldwell, J. W.; Kollman, P. A.; Case, D. A. Development and Testing of a General Amber Force Field. *J. Comput. Chem.* **2004**, *25*, 1157−1174.
(27) Jorgensen, W. L.; Chandrasekhar, J.; Madures, J.; Impey, R. W.; Klein, M. L. Comparison of Simple Potential Functions for Simulating Liquid Water. *J. Chem. Phys.* **1983**, *79*, 926−935.
(28) Ryckaert, J. P.; Ciccotti, G.; Berendsen, J. C. Numerical Integration of the Cartesian Equations of Motion of a System with Constrains: Molecular Dynamics of N-alkanes. *J. Comput. Phys.* **1977**, *23*, 327−341.
(29) Darden, T.; York, D.; Pedersen, L. Particle mesh Ewald (PME): A log (N) Method for Ewald Sums in Large systems. *J. Chem. Phys.* **1993**, *98*, 10089−10092.
(30) Fogolari, F.; Brigo, A.; Molinari, H. Protocol for MM/PBSA Molecular Dynamics Simulations of Proteins. *Biophys. J.* **2003**, *85*, 159−166.
(31) Kollman, P. A.; Massova, I.; Reyes, C.; Kuhn, B.; Huo, S.; Lee, M.; Lee, T.; Duan, Y.; Wang, W.; Donini, O.; et al. Calculating Structures and Free Energies of Complex Molecules: Combining Molecular Mechanics and Continuum Models. *Acc. Chem. Res.* **2000**, *33*, 889−897.
(32) Massova, I.; Kollman, P. A. Combined Molecular Mechanical and Continuum Solvent Approach (MM-PBSA/GBSA) to Predict Ligand Binding. *Perspect. Drug Discovery Des.* **2000**, *18*, 113−135.
(33) Wang, J.; Morin, P.; Wang, W.; Kollman, P. A. Use of MM-PBSA in Reproducing the Binding Free Energies to HIV-1 RT of TIBO Derivatives and Predicting the Binding Mode to HIV-1 RT of Efavirenz by Docking and MM-PBSA. *J. Am. Chem. Soc.* **2001**, *123*, 5221−5230.
(34) Cheatham, T. E., III; Srinivasan, J.; Case, D. A.; Kollman, P. A. Molecular Dynamics and Continuum Solvent Studies of the Stability of PolyG-PolyC and PolyA-PolyT DNA Duplexes in Solution. *J. Biomol. Struct. Dyn.* **1998**, *16*, 265−280.
(35) Kuhn, B.; Kollman, P. A. Binding of a Diverse Set of Ligands to Avidin and Streptavidin: An Accurate Quantitative Prediction of their Relative Affinities by a Combination of Molecular Mechanics and Continuum Solvent Models. *J. Med. Chem.* **2000**, *43*, 3786−3791.
(36) Gilson, M. K.; Sharp, K. A.; Honig, B. H. Calculating the Electrostatic Potential of Molecules in Solution: Method and Error Assessment. *J. Comput. Chem.* **1988**, *9*, 327−335.

(37) Tsui, V.; Case, D. A. Theory and Applications of the Generalized Born Solvation Model in Macromolecular Simulations. *Biopolymers* **2001**, *56*, 275−291.
(38) Still, W. C.; Tempczyk, A.; Hawley, R. C.; Hendrickson, T. Semianalytical Treatment of Solvation for Molecular Mechanics and Dynamics. *J. Am. Chem. Soc.* **1990**, *112*, 6127−6129.
(39) Weiser, J.; Shenkin, P. S.; Still, W. C. Approximate Atomic Surfaces from Linear Combinations of Pairwise Overlaps (LCPO). *J. Comput. Chem.* **1999**, *20*, 217−230.
(40) Manas, E. S.; Unwalla, R. J.; Xu, Z. B.; Malamas, M. S.; Miller, C. P.; Harris, H. A.; Hsiao, C.; Akopian, T.; Hum, W. T.; Malakian, K.; et al. Structure-Based Design of Estrogen Receptor-β Selective Ligands. *J. Am. Chem. Soc.* **2004**, *126*, 15106−15119.